THE ASTROPHYSICAL JOURNAL, 568:L61–L65, 2002 March 20

CORRELATED DYNAMICS OF HOT AND COOL PLASMAS IN THE MAIN PHASE OF A SOLAR FLARE

B. KLIEM,[1] I. E. DAMMASCH,[2] W. CURDT,[2] AND K. WILHELM[2]

Received 2001 September 7; accepted 2002 February 8; published 2002 February 22

ABSTRACT

We report far-ultraviolet observations of a solar limb flare obtained by the Solar Ultraviolet Measurements of Emitted Radiation (SUMER) spectrometer. At a fixed pointing of the slit above the limb, spectra were simultaneously obtained in several emission lines that covered a wide temperature range from $\approx 10^4$ to $\approx 10^7$ K. The temporal evolution of the spectra revealed, for the first time, a high degree of correlation between the dynamical behavior of hot ($T \sim 10^7$ K) and cool ($T \sim 10^4$ K) coronal material during the main phase of a flare. We note that the data did not show any indication of the presence of a prominence. Hot and cool plasmas brightened at nearly the same location. Their Doppler shifts, which were opposite to each other, reached peak values simultaneously. Thereafter, the two components showed anticorrelated, rapidly damped, and oscillatory Doppler shifts and a very similar decay of the line widths, but with the cool plasma reaching maximum brightness before the hot plasma. This behavior points to an active role for cool plasma in the dynamics of this flare, different from the usual picture of passive cooling after the impulsive phase. We suggest a model in which the localized cooling of coronal plasma by the thermal instability triggers magnetic reconnection through the resulting enhanced resistivity, the combined processes leading to the correlated dynamics of hot and cool plasmas in a loop-loop interaction geometry.

Subject headings: MHD — plasmas — Sun: corona — Sun: flares — Sun: UV radiation

1. INTRODUCTION

The impulsive release of magnetically stored energy in solar flares involves plasma heating to temperatures of (1–3) × 10^7 K, the acceleration of hot plasmas, and the acceleration of energetic particles. Except for the possible eruption of a prominence, "cool" material ($T \ll 10^6$ K) is usually thought to participate in the flare process only *after* the impulsive energy release and heating, emerging from the cooling of dense, hot flare loops in the main flare phase (e.g., Tandberg-Hanssen & Emslie 1988). This basically passive role of cool plasma in flares is suggested by Hα observations that show so-called *postflare* loops in arcade flares at the limb and arch filament systems in flares on the disk, also forming after the impulsive phase (e.g., Schmieder 1992). Heated chromospheric plasma plays an important role in the flare dynamics by providing the link between the initial impulsive energy release and the formation of *dense*, hot flare loops. This "chromospheric evaporation" was recently confirmed by spatially resolved EUV spectroscopy in coronal and transition region lines during the late phase of a flare on the disk (Czaykowska et al. 1999).

In this Letter, we present one of the first spectrally and (in one dimension) spatially resolved UV observations of a limb flare, in which cool plasma is seen free of the chromospheric background. The data show near-simultaneous brightenings and line broadenings and the correlated oscillatory motions of hot (10^7 K) and cool (2×10^4 K) plasmas, which are not related to a prominence, indicating a more active role than generally thought for cool plasma in the dynamical evolution of this flare.

2. OBSERVATIONS

The Solar Ultraviolet Measurements of Emitted Radiation (SUMER) spectrometer (Wilhelm et al. 1995) on board the *Solar and Heliospheric Observatory* (*SOHO*) observed a C4.6 flare in NOAA Active Region 8758 at the northeast limb on 1999 November 6 after ≈06:30 UT. The flare occurred during a time series taken at a fixed slit position above the limb. In the time series, eight spectral windows were simultaneously read out with 120 s cadence, interrupted after blocks of 25 exposures by three full detector readouts with 320 s cadence. The spectral windows, 2 Å wide, were selected from the range 1325–1360 Å and centered at emission lines that cover a wide temperature range. The time series was preceded and followed by a raster scan, providing an image in the line He I λ584.3 formed at $T \approx 2 \times 10^4$ K. The $300'' \times 1''$ slit, detector A, and the full spatial resolution ($1''$ pixels) were used. Standard methods were applied to correct the raw data for dead-time and gain effects and detector distortions (see, e.g., Dammasch et al. 1999). In addition to the SUMER data, series of images taken by the EUV Imaging Telescope (EIT) on *SOHO* in the Fe XII line at 195 Å with a cadence between 6 and 17 minutes and by the soft X-ray telescope (SXT) on *Yohkoh* with 6–16 s cadence are available.

The event under consideration occurred ≈12.5 hr after an M3 flare in the same active region, which had led to the formation of a prominent arcade of postflare loops (best displayed in an 171 Å image taken by the *Transition Region and Coronal Explorer* [*TRACE*] at 02:22 UT; see Fig. 3*c* in Aschwanden, Nightingale, & Alexander 2000). In the EIT images, the arcade was seen to rise until about 04:00 UT; thereafter, it stayed approximately constant in size and shape for several hours.

The flare at ≈06:30 UT did not lead to major changes in the arcade. In the EIT images, it caused a strong brightening at the southern footpoints of the arcade (with no measurable effect at the northern footpoints) and a weak brightening in the corona just inside the arcade also close to its southern footpoints (Figs. 1*a* and 1*b*). This coronal brightening was present only in the image taken at the time of peak soft X-ray flux. It included two or three smaller loops whose narrow shapes indicate that they were strongly rotated with respect to the main part of the arcade, which appeared to lie nearly in the plane of the sky.

Similar to the EUV brightening, the soft X-ray brightening also consisted of two main components, both at the southern

[1] Astrophysikalisches Institut Potsdam, An der Sternwarte 16, D-14482 Potsdam, Germany; bkliem@aip.de.
[2] Max-Planck-Institut für Aeronomie, D-37191 Katlenburg-Lindau, Germany.

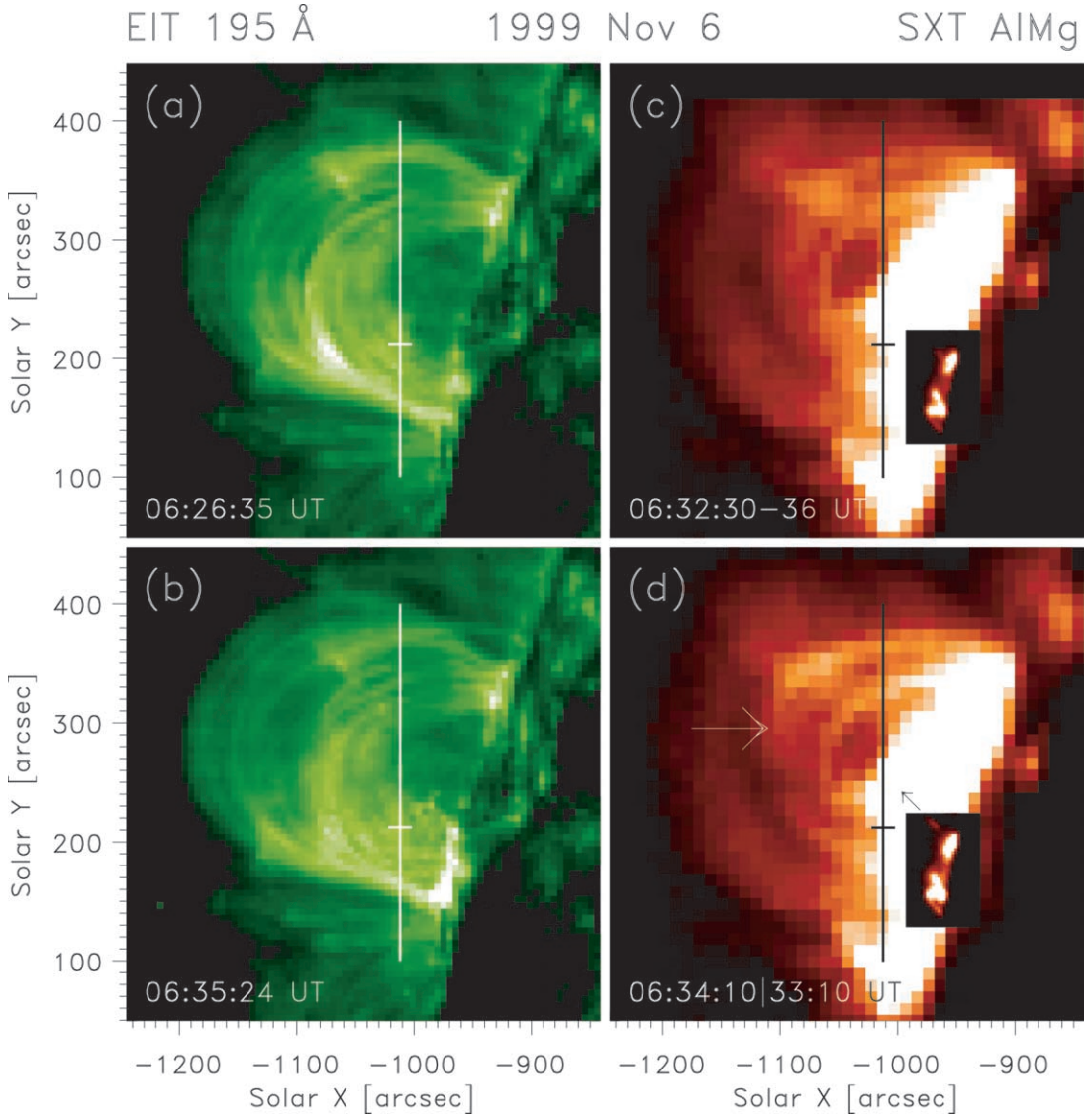

FIG. 1.—(*a*, *b*) The two EIT images closest in time to the flare peak (5.″24 pixel^{-1} resolution). The SUMER slit position during the time series and the position of the flare-related C II brightening (≈40,000 km above the photosphere) are indicated. (*c*, *d*) First and last SXT quarter-resolution images (9.″8 pixel^{-1}) of the *Yohkoh* observation sequence. Part of the full-resolution images (2.″45 pixel^{-1}) are inserted: a near-simultaneous image in (*c*) and the image showing the weak ejection at peak intensity in (*d*). The rising X-ray loop is marked by a large arrow, and the direction of the weak ejection is shown by a small arrow.

footpoints of the arcade (Figs. 1*c* and 1*d*). The stronger (southern) source was nearly coincident with the strongest EUV brightening (Fig. 1*b*) and marked the footpoint of a hot loop that ascended during the flare with a projected velocity of ≈90 km s^{-1} (whereas the two neighboring soft X-ray loops stayed constant in shape). This loop did not have a clear counterpart in the EIT images. The slightly weaker northern source appeared at the footpoints of the weak coronal brightening seen by EIT. It gave rise to a small bloblike ejection ascending at a projected velocity of ≈190 km s^{-1} into a direction northward of the main effects at the SUMER slit and fading early in the event (≈06:33:30 UT) about halfway between the photosphere and the slit position; the existence of a direct relationship between the ejection and the effects seen by SUMER is therefore questionable. The two SXT sources had different light curves, suggesting that they were formed in different magnetic structures (see Fig. 3*b* below).

The EIT and SXT data suggest that the flare was caused by interactions between a small number of loops near the southern footpoints of the preexisting and essentially stable arcade; however, due to the limited resolution, no clear-cut image of the morphology can be derived.

The two SUMER images taken in the He I line show a system of cool postflare loops essentially cospatial with the arcade seen in the EIT images. There is no indication of a prominence. Also, the EUV images closest in time to the flare (EIT 304 Å at 03:17 UT and *TRACE* 171 and 1600 Å at 05:01 UT) did not show any signature of a prominence near the southern footpoints of the arcade. Figure 2 presents the SUMER He I images along with three blocks of the time series data that include the flare. Three lines were selected: a representative "cool" line (C II λ1335.7 formed at $T_e \approx 2 \times 10^4$ K), a line formed at typical coronal temperatures (Fe XII λ1349.4), and a representative "hot" line (Fe XXI λ1354.1 formed at $T_e \approx 10^7$ K). Lines formed at similar temperatures (S I and C I for cool plasma and Cr XVIII, Fe XIX, and Fe XX for hot plasma) showed a similar behavior (see Feldman et al. 1997, 2000 for line identifications).

The time series data show a marked brightening of the Fe XXI line during ≈06:30–07:10 UT, which is the most direct signature of the flare energy release contained in the SUMER data. The main enhancement occurred near 220″ north close to the position of the weak coronal brightening seen by EIT, i.e., closer to the

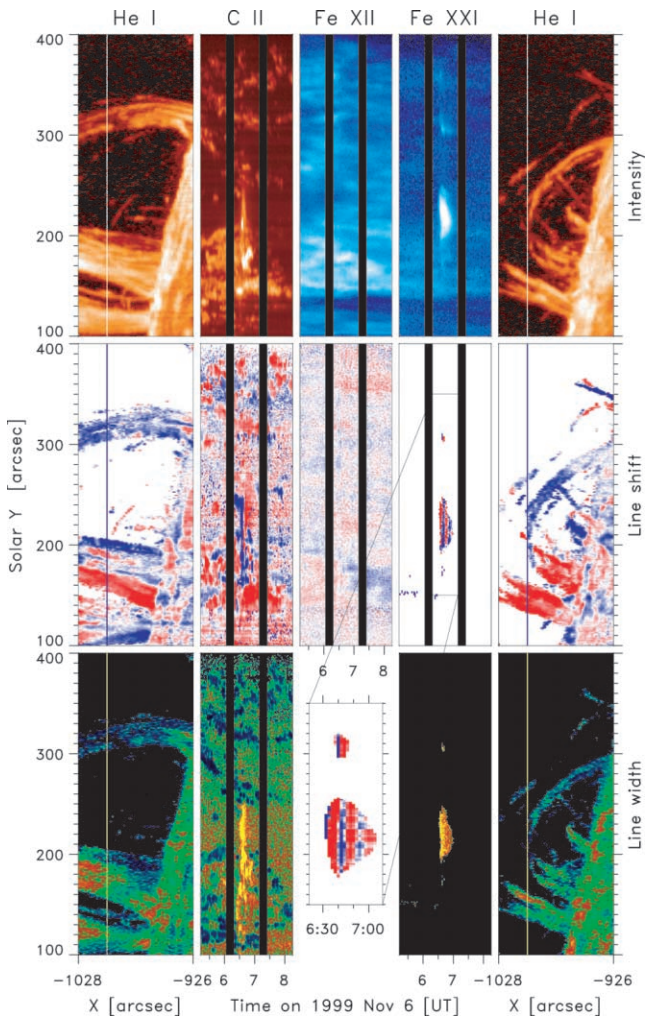

FIG. 2.—*Top row:* He I images of the active region obtained from the initial (00:33–47 UT) and final (09:41–55 UT) SUMER raster scans and line-integrated intensity time series at a fixed slit position (1012″ east, indicated in the images) in the C II, Fe XII, and Fe XXI lines. All intensities are plotted at logarithmic scales. *Middle row:* Line shifts. *Bottom row:* Line widths. Shifts and widths of the Fe XXI line were determined only above a certain flux level, in order to avoid confusion from an unidentified line blend at 1353.62 Å (see Feldman et al. 1997). Instead of the nearly structureless plot of the Fe XII line widths, the bottom row shows a zoom of the Fe XXI line shifts obtained after applying a running average to the spectra including ± 10 pixels in solar Y and ± 1 pixel in λ.

weaker of the two main soft X-ray brightenings. Two secondary Fe XXI enhancements with peak fluxes lower than that of the main enhancement by factors of 40 and 70 occurred near 300″ and 360″ north, respectively. The SUMER slit crossed the rising soft X-ray loop at 360″ north, but the other secondary Fe XXI enhancement had no clear counterpart in the SXT data.

The lines formed at typical coronal temperatures (Fe XII, Ar XII, Si IX, and Al X) did not show any obvious enhancements, shifts, or broadenings related to the flare. This indicates (1) that the plasma involved in the flare process had a small filling factor relative to the column density of the coronal material sampled by 1 SUMER pixel and (2) that the weak coronal brightening in the EIT image at 06:35:24 UT was caused by emission in the Ca XVII or Fe XXIV lines, which fall in the passband at 195 Å.

Enhancements in C II occurred intermittently throughout the whole time series. Such timescale variability (in the range of minutes) of coronal plasma at $T \lesssim 10^5$ K was studied by Kjeldseth-Moe & Brekke (1998) and Schrijver (2001) and is probably due to locally and temporarily enhanced cooling. Two C II enhancements were correlated with the flare signatures of hot plasma. The short northern C II enhancement at ≈210″ north was nearly coincident with the main Fe XXI enhancement and the weak coronal EIT brightening. It showed a particularly impulsive rise and had a weak tail up to ≈240″ north, i.e., about the same extension along the slit as the Fe XXI enhancement. The southern C II enhancement at ≈170″ north had only a very weak counterpart in Fe XXI but was coincident with the intersection of the slit with the rising soft X-ray loop. No C II enhancements could be detected at the place of the two weak secondary Fe XXI enhancements.

Figure 3*a* shows the spatial and temporal relationship between the flare-related enhancements in hot (Fe XXI) and cool (C II) lines at the position of the SUMER slit (zoomed time series data). The temporal evolution of the UV flux is plotted in Figure 3*b* along with X-ray light curves, observed by the *Geostationary Operational Environmental Satellite* (*GOES*) and the SXT and the hard X-ray telescope (HXT) on board *Yohkoh*. The Fe XXI flux started to rise between 06:31 and 06:33 UT—simultaneous with the onset of the impulsive flare phase (to within the time resolution of 2 minutes). However, the main rise of the Fe XXI and C II flux in the range 200″–240″ north occurred 4 minutes later, at the end of the impulsive phase. This indicates that the SUMER slit was pointed close to but not exactly at the site of the primary impulsive energy release and that the hot and cool plasmas were guided toward the slit position by *the same* magnetic structure. The C II enhancement near 170″ north showed a slightly delayed onset and a different decay profile. It is important to note that both C II enhancements peaked *before* the maximum of the Fe XXI enhancement and that the cospatial C II enhancement decayed *earlier* than the Fe XXI enhancement.

The shifts and the widths of both lines are plotted in Figures 3*c* and 3*d*, respectively. The variations of the shifts and widths of the Fe XXI line were coherent over the full extent of the main Fe XXI enhancement. It was thus possible to take a running average for this line over ± 10 spatial and ± 1 spectral pixels without smearing significantly the values of the shift and width. This enabled us to determine unambiguously the spectral shape, line shift, and line width for Fe XXI from the beginning of the enhancement. The Fe XXI enhancement at 06:32 UT was composed of several components (the number varying between two and five along the slit) that were blueshifted on average and possessed a high total spectral width. At 06:34 UT, an additional redshifted component of slightly higher intensity occurred, turning the average shift into red and leading to a maximum total line width. This new component grew and dominated the line profile during the subsequent exposures ($t \geq$ 06:36 UT). It first showed a strong redshift (06:36–38 UT), followed by three reversals of the line shift with a timescale of 4–8 minutes that resemble a strongly damped oscillation. The C II line showed a strong blueshift, which peaked simultaneously with the strong redshift of Fe XXI. A subsequent oscillation of the C II line shift with a similar timescale as the Fe XXI shift but opposite sign is also indicated by the spectra. Both lines showed a maximum shift before maximum flux. The peak cross-correlation coefficient of the Fe XXI and C II line shift profiles is -0.93 at zero time lag between 06:34 and 07:10 UT and -0.82 at a 2 minute time lag between 06:40 and 07:10 UT. Both lines reached substantial excess (turbulent) line widths at the onset of the flux enhancements, followed by a very similar decay. The close spatial and temporal association between these Fe XXI and C II enhancements, the presence of highly correlated oscillatory flows, and the similar temporal evolution of the line widths leave no doubt that the dynamical

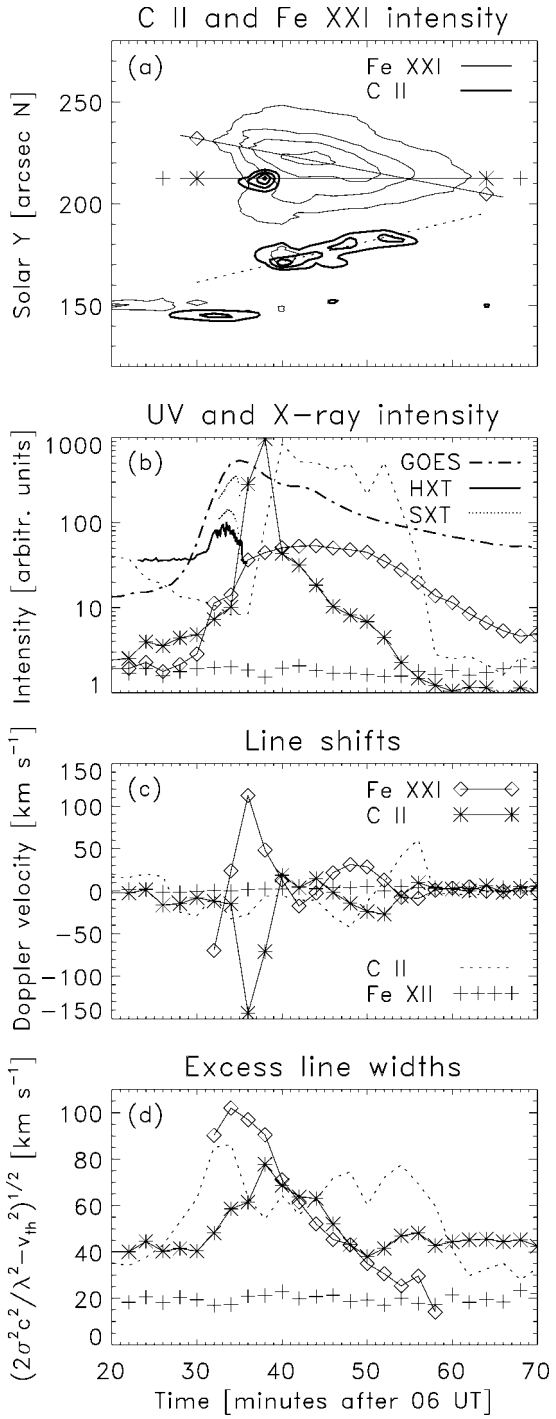

FIG. 3.—(*a*) Equidistant isocontours of line-integrated intensity (linear scale, 20%–92% of maximum) showing the flare-related brightenings in Fe XXI (*light contours*) and C II (*heavy contours*). Cut lines, along which the time profiles are plotted in (*b*)–(*d*), are indicated. (*b*) Time profiles of line-integrated UV intensity, of the *GOES* 0.5–4 Å flux, of the *Yohkoh* HXT 14–23 keV flux, and of the two footpoint sources resolved by *Yohkoh* SXT. C II and Fe XII intensities are in units counts pixel^{-1} s^{-1}; the X-ray and Fe XXI intensities were scaled to fit into the figure. *Yohkoh* orbital night time occurred after 06:35 UT. The weaker northern SXT footpoint source peaked at 06:33:30 UT, ≥70 s earlier than the southern footpoint source. (*c*) Line shifts relative to the average preflare line positions. (*d*) Excess line widths, where σ is the standard deviation of a Gaussian fit (which underestimates the true width of the Fe XXI line becaue of the presence of non-Gaussian tails) and v_{th} is the thermal velocity of the ion. Fe XXI data were extracted from the spectra after applying a running average, including ±2 pixels in solar *Y* and ±1 pixel in λ for (*a*) and (*b*) and ±10 pixels in solar *Y* and ±1 pixel in λ for (*c*) and (*d*). SUMER data points are plotted at the center of each exposure interval.

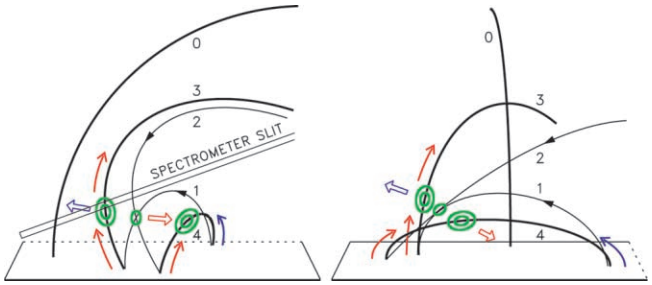

FIG. 4.—Front and side view of the suggested condensation-reconnection geometry. Magnetic reconnection between loops 1 and 2 is triggered by a condensation (*green contour*) at their point of contact. The resulting loops 3 and 4 carry away the remainders of the (grown) condensation at the end of the process. The main arcade is indicated by loop 0. Open arrows show reconnection outflows, and solid arrows show evaporation upflows; their color (*red/blue*) indicates the direction of the Doppler shift. The upward-directed reconnection outflow is seen blueshifted (Fe XXI at 06:32 UT and C II at 06:36–38 UT). The upward-directed flow of evaporated (hot) chromospheric plasma in loop 3 is seen redshifted (Fe XXI at 06:34–38 UT).

evolution of hot and cool plasmas was closely coupled in this part of the flare.

At the position of the southern C II enhancement (≈170″ north), all data sets show characteristics that differ qualitatively from those at the northern C II enhancement (≈210″ north). In the following discussion, we will therefore assume that the two structures flared essentially independently of each other and will concentrate on the correlated behavior of hot and cool plasmas at the main Fe XXI and northern C II enhancements.

3. DISCUSSION

The classical model of arcade flares after Kopp & Pneuman (1976) predicts the formation of cool postflare loops (by radiative and conductive cooling) *inside* of dense hot flare loops and a continuous reformation of this double structure at permanently increasing heights. This model is clearly inconsistent with the SUMER observations of a C II enhancement that *preceded* a nearly cospatial Fe XXI enhancement in peak and decay time. (The delayed main rise of the Fe XXI and C II emissions in the SUMER data implies in this model that the slit was pointed above the starting height of flare loop formation.)

We consider the alternative model of loop-loop interaction (e.g., Nishio et al. 1997; Hanaoka 1997). Noting the strong temperature dependence of the electrical resistivity, $\eta \propto T^{-3/2}$, which implies that η rises by a factor of $\sim 10^3$ if the temperature drops from coronal to upper chromospheric values, we suggest that a condensation formed by the thermal instability (e.g., in a density enhancement between two approaching magnetic loops) may trigger magnetic reconnection. The presence of dense and already cooling material from the preceding M3 flare may have supported such an evolution in the flare under consideration.

A sketch of a configuration consistent with this assumption and the spectral data is given in Figure 4. This geometry is suggested by taking the following considerations into account: (1) The condensation crossed the slit at the time of peak C II flux (06:38 UT). (2) Therefore, it had a bulk line-of-sight velocity of ≈−70 km s^{-1}. (3) Consequently, the C II peak line shift at 06:36 UT shows plasma streaming *away* from the condensation—obviously with the reconnection outflow. Continued inflow into an ongoing condensation process, a potential candidate for the explanation of opposite flows, is not apparent in the data. (4) It appears plausible to assume that the formation of the condensation and the reconnection of the loops had essentially fin-

ished by 06:36–38 UT (the end of the impulsive phase) and that the remainders of the condensation were then swept away by the newly formed loops. (5) The upward-directed reconnection outflow had a blue Doppler shift (Fe XXI at 06:32 UT and C II at 06:36–38 UT) if the reconnected loop 3 moved toward the observer. This is the case if the original loops were appropriately oriented, particularly if loop 2 was strongly tilted away from the observer (an effect resulting from internal twist; e.g., Amari et al. 1996) so that the reconnected and presumably less twisted loop 3 was less tilted. The *TRACE* images suggest such an orientation for loop 2 (see Fig. 3*c* in Aschwanden et al. 2000). Then the upward-directed flow of evaporated (hot and dense) chromospheric plasma had a red Doppler shift left of the apex of loop 3 (Fe XXI at 06:34–38 UT). (6) We assume that the approximate agreement of the absolute values of the Fe XXI and C II peak Doppler velocities is a coincidence.

Based on our assumption, the opposite flows of hot and cool plasmas between 06:32 and 06:40 UT can be explained by an interaction between a single pair of loops or loop bundles. The trivial possibility that interactions between several differently oriented loops (or loop bundles) led to the opposite flows is not excluded, but it does not naturally explain the high correlation of the observed line shifts and widths. The Fe XXI spectra contained several blueshifted components at the onset of the event (06:32–34 UT), indicative of several interacting loops, but the strong enhancements of both lines at later times were always clearly dominated by only one component. Explanations of the main flows in terms of an untwisting eruptive filament or in terms of a condensation at the head of the reconnection outflow (Innes & Tóth 1999) are in conflict with the opposite sign of the cool and hot line shifts. A transverse oscillation of a pair of loops containing cool and hot plasmas and oscillating in antiphase (as in the event described by Schrijver & Brown 2000) can also nearly certainly be ruled out for this phase because it would imply an unreasonable total displacement of the loops ($\geq$27,000 km) occurring at a height of only $\approx$40,000 km. This exceeds the largest displacements detected so far in *TRACE* data of 17 events (Aschwanden et al. 2002) by a factor of 3.

The further reversals of the Fe XXI and C II line shifts after 06:40 UT do not directly follow from the model, but they are consistent with a relaxation oscillation in this configuration. For example, the amplitudes, periods, and damping timescales possess values typical of transverse postflare loop oscillations observed by *TRACE*. SUMER data of such oscillations will be the subject of future investigations; here we note only that the substantial instantaneous range along the slit of coherent line shift oscillations favors an interpretation in terms of impulsively generated propagating MHD waves (Aschwanden et al. 2002) above interpretations as standing kink modes in isolated loops. Alternatively, also relaxation oscillations of flows along the reconnected field lines, caused by strongly asymmetric chromospheric evaporation due to an asymmetric reconnection point, are conceivable.

From the emission measure of the C II emission, $\sim 10^{45}$ cm^{-3}, and with an assumed size of $(10'')^3$, one finds an average density $n_{\mathrm{C\,II}} \sim 5 \times 10^{10}$ cm^{-3} and a total electron number of up to $N_{\mathrm{tot}} \sim 10^{37}$ in the condensation. The presence of a condensation at the reconnection site may thus help us solve the electron number problem of particle acceleration in flares (see, e.g., Miller et al. 1997).

We thank D. E. McKenzie and J. Sato for providing us with reduced *Yohkoh* data and the anonymous referee, K. Muglach, M. J. Aschwanden, and E. Landi for very helpful comments. The EIT, SXT, and HXT data are courtesy of the *SOHO* EIT and the *Yohkoh* SXT and HXT consortiums, respectively. The SUMER project is financially supported by DLR, CNES, NASA, and the ESA PRODEX programme. The work of B. K. was also supported by the EU under contract HPRN-CT-2000-00153.

REFERENCES

Amari, T., Luciani, J. F., Aly, J. J., & Tagger, M. 1996, ApJ, 466, L39
Aschwanden, M. J., De Pontieu, B., Shrijver, C. J., & Title, A. 2002, Sol. Phys., 206, 99
Aschwanden, M. J., Nightingale, R. W., & Alexander, D. 2000, ApJ, 541, 1059
Czaykowska, A., de Pontieu, B., Alexander, D., & Rank, G. 1999, ApJ, 521, L75
Dammasch, I. E., Wilhelm, K., Curdt, W., & Hassler, D. M. 1999, A&A, 346, 285
Feldman, U., Behring, W. E., Curdt, W., Schuehle, U., Wilhelm, K., Lemaire, P., & Moran, T. M. 1997, ApJS, 113, 195
Feldman, U., Curdt, W., Landi, E., & Wilhelm, K. 2000, ApJ, 544, 508
Hanaoka, Y. 1997, Sol. Phys., 173, 319
Innes, D., & Tóth, G. 1999, Sol. Phys., 185, 127
Kjeldseth-Moe, O., & Brekke, P. 1998, Sol. Phys., 182, 73
Kopp, R. A., & Pneuman, G. W. 1976, Sol. Phys., 50, 85
Miller, J. A., et al. 1997, J. Geophys. Res., 102, 14,631
Nishio, M., Yaji, K., Kosugi, T., Nakajima, H., & Sakurai, T. 1997, ApJ, 489, 976
Schmieder, B. 1992, in Eruptive Solar Flares, ed. Z. Švestka, B. V. Jackson, & M. E. Machado (Berlin: Springer), 124
Schrijver, C. J. 2001, Sol. Phys., 198, 325
Schrijver, C. J., & Brown, D. S. 2000, ApJ, 537, L69
Tandberg-Hanssen, E., & Emslie, A. G. 1988, The Physics of Solar Flares (Cambridge: Cambridge Univ. Press)
Wilhelm, K., et al. 1995, Sol. Phys., 162, 189